Asociación Argentina
de Mecánica Computacional

Mecánica Computacional Vol XLI, pp. 375-384
C.I. Pairetti, M.A. Pucheta, M.A. Storti, C.M. Venier (Eds.)
H. Castro, J. D'Elía, L. Battaglia, M. Coussirat, S. Sarraf, A. Scarabino (Issue eds.)
Rosario, November 5-8, 2024

COMPUTATIONAL ANALYSIS OF WIND NEIGHBORHOOD EFFECTS ON BUILDINGS: A COMPARISON BETWEEN CLOSURE MODELS FOR TURBULENCE

Paulo U. Silva[a], **Gustavo Bono**[b], **Marcelo Greco**[a]

[a]*Departamento de Engenharia de Estruturas, Escola de Engenharia, Universidade Federal de Minas Gerais, Avenida Presidente Antônio Carlos, 6627, CEP 31270-901, Belo Horizonte, Minas Gerais, Brazil, pauloulisses@ufmg.br, mgreco@dees.ufmg.br*

[b]*Laboratório de Engenharia Computacional, Centro Acadêmico do Agreste, Universidade Federal de Pernambuco, Av. Marielle Franco, s/n, KM 59, Nova PE, CEP 50104-900, Caruaru, Pernambuco, Brasil, gustavo.bono@ufpe.br*

Keywords: Computational fluid dynamics, aerodynamic coefficients, RANS, OpenFOAM

Abstract. Determining the neighboring effects of wind is a complex task, as generic approaches are often unable to accurately capture the interactions between buildings and their surrounding environment. For this reason, standard guidelines may be insufficient for determining these effects, making it necessary to rely on wind tunnel testing or numerical simulations through computational fluid dynamics (CFD). This study presents an analysis of the changes in aerodynamic coefficients of the CAARC (Commonwealth Advisory Aeronautical Research Council) building due to the presence of neighboring structures that interfere with wind flow. The neighborhood consists of eight blocks with proportions of 1:1:3. Turbulence was modeled using the Reynolds-Averaged Navier-Stokes (RANS) approach, employing the $k-\epsilon$ and $k-\omega$ SST turbulence closure models. A comparative analysis of the results obtained from these two models is presented. The study was conducted by varying the system's orientation from 0 to 90 degrees in 15-degree intervals. Results show that the perimeter buildings create a shielding effect on the centrally located CAARC building, leading to a reduction in the drag coefficient. Additionally, for some angles, the presence of neighboring structures caused an increase in the torsional and lift coefficients.

ISSN: 2591-3522 DOI: 10.70567/mc.v41i7.37

1 INTRODUCTION

The action of wind in urban areas is a field of great interest for the construction industry, as the effects of this type of demand have a major impact on the comfort of occupants and pedestrians, in addition to affecting the safety and durability of structural elements. As seen in the work of Razak *et al.* (2013), in regions with a high density of buildings, the complexity of wind flow increases due to the interference that the set of buildings causes in the wind flow profile. Wind engineering plays an important role in the development of urban infrastructure, especially in regions with many buildings. It involves the study and analysis of the effects of wind on buildings and their surroundings, with the aim of ensuring structural safety and pedestrian comfort (Blocken *et al.*, 2012). In regions with a high density of tall buildings, the intensity of wind turbulence increases significantly, causing impacts on structural systems and the environment at pedestrian level (Aristodemou *et al.*, 2018).

Studies in this area focus on several aspects, such as the evaluation of wind-induced forces and moments (Lin *et al.*, 2005), wind flow topology around structures at ground level for pedestrian comfort (Blocken *et al.*, 2016), and the measurement of wind pressure coefficients on building surfaces (Meng *et al.*, 2018). Wind tunnel tests and computational fluid dynamics (CFD) simulations are the most common methodologies for analyzing this type of system.

One of the most important points is the study of interference effects between buildings, especially in the presence of tall buildings. Ishida *et al.* (2023) and Ishida *et al.* (2024), for example, evaluate through wind tunnel tests and the CFD Large-Eddy Simulations (LES) methodology how the presence of a tall structure can modify the flow topology and velocity field, influencing adjacent buildings. Furthermore, densely built urban areas tend to form channels for wind flow, creating high-speed zones that can impair pedestrian comfort.

As seen in Iqbal and Chan (2016), the presence of buildings modifies the wind profile, altering the pressures on adjacent buildings. This interference phenomenon changes the forces acting on neighboring structures, making it necessary to carry out a wind engineering study during the design phase to understand how the building will be affected by its surroundings, and how it will affect them. Some of the main effects caused are the induction of vibrations that may coincide with natural modal frequencies, increased moment and drag coefficients, and consequentially, lateral, and torsional displacements (Thepmongkorn *et al.*, 2002).

In this work, the effects of neighborhood interference on the aerodynamic coefficients of a CAARC-type tall building are evaluated by varying the wind incidence angle through CFD in the RANS turbulence models through the open-source software OpenFOAM. Section 2 presents the equations of the turbulence model and the possible closure methods. Section 3 shows the methodology for modeling the atmospheric boundary layer (ABL), initial conditions and inlet conditions in the domain for the computational simulations. Section 4 presents the validation of the simulation model, using the example of the flow around a cube. Section 5 presents the results of the study and, finally, the final considerations and potential developments of the current work are presented in Section 6.

2 RANS MODEL

The central idea of the Reynolds-averaged Navier-Stokes (RANS) equations is Reynolds decomposition (Reynolds, 1895), whereby the flow quantities are decomposed into their time-averaged and fluctuating components. Since the turbulence problem is nonlinear, the average equations are associated with turbulent fluctuations in velocity and pressure fields, producing Reynolds stresses (Andersson *et al.*, 2012). Considering an incompressible Newtonian fluid and a steady flow, the RANS model is described by the set of partial differential equations described by Eq. (1),

$$\rho \bar{u}_j \frac{\partial \bar{u}_i}{\partial x_j} = \rho \bar{f}_i + \frac{\partial}{\partial x_j}\left[-\bar{p}\delta_{ij} + \mu\left(\frac{\partial \bar{u}_i}{\partial x_j} + \frac{\partial \bar{u}_j}{\partial x_i}\right) - \rho\overline{u_i' u_j'}\right] \tag{1}$$

where ρ is the specific mass of the fluid, $\bar{u}_i$ and $\bar{u}_j$ represent the average velocity components, x_i and x_j are the Cartesian directions orthogonal to each other, $\bar{f}_i$ is the average set of forces per unit mass, $\bar{p}$ is the average set of pressures, δ_{ij} is the Kronecker delta, and μ is the molecular viscosity of the fluid. On the left side of the equation, the change in the average momentum of a fluid element due to the instability in the mean flow and convection by the mean flow are presented. The change is balanced by the average body force, the isotropic stress, the viscous stress, and the Reynolds stress. This set of equations is highly complex and requires the use of closure models to obtain the flow response.

The resolution is done by turbulence closure models. In this work, two numerical configurations are used to simulate turbulent flow, the classic $k - \epsilon$ and $k - \omega$ Shear Stress Transport (SST) closure models. The resolution of the RANS models equations is associated with the determination of the Turbulent Kinetic Energy (TKE), denoted by k, for each time step of the simulation. TKE is defined as the average kinetic energy per unit mass associated with the turbulent flow vortices (Dondapati and Rao, 2013), and their dissipation. Eq. (2) presents the analytical differential equation for TKE,

$$\frac{Dk}{Dt} + \nabla \cdot T' = P - \epsilon \tag{2}$$

where Dk/Dt is the mean material derivative of TKE, $\nabla \cdot T'$ is the turbulence transport of TKE and P and ϵ are the rates of production and dissipation of TKE.

The TKE dissipation, denoted as ϵ, and the specific dissipation, denoted as ω must be determined to solve the differential equations associated with the turbulence problem. ϵ is analytically calculated as the inner product of the velocity gradient multiplied by the kinematic viscosity of the fluid ν, as presented in Eq. (3). Variable ω is calculated by normalizing ϵ by the TKE and a constant $C_\mu = 0.09$, associated with the $k - \omega$ modeling, as presented by Eq. (4).

$$\epsilon = \nu\left\{\left\langle\frac{\partial u_i}{\partial x_j} + \frac{\partial u_j}{\partial x_i}\right\rangle\left\langle\frac{\partial u_i}{\partial x_j} + \frac{\partial u_j}{\partial x_i}\right\rangle\right\} \tag{3}$$

$$\omega = \frac{\epsilon}{k C_\mu} \tag{4}$$

3 METHODOLOGY

The simulations of this work were performed in OpenFOAM v10 (https://openfoam.org/version/10/). This section presents the modeling of the simulation domain, flow inlet, boundary, and initial conditions for the problems.

3.1 Simulation domain

The domain was discretized according to the recommendations of Franke *et al*. (2004) and Tominaga *et al.* (2008), which establish guidelines for flow around buildings in CFD simulations with high Reynolds number. The building with X:Y:Z proportions (base, width, height) and its surroundings are positioned at a distance of 5Z from the upstream face, side faces and top of the domain and 15Z from the downstream face, as illustrated by Figure 1.

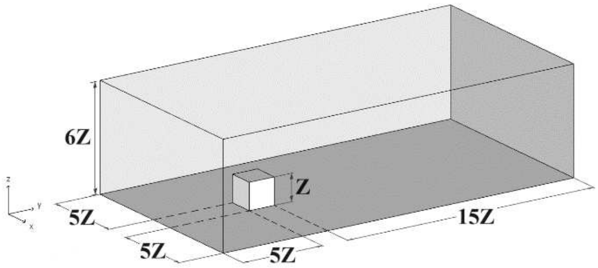

Figure 1: Simulation domain.

3.2 Boundary and initial conditions

The flow was modeled to simulate the ABL according to a logarithmic function, as seen in van Doormal and Raithby (1984), Richards and Hoxey (1993) and Hargreaves and Wright (2007). The reference velocity and height are, respectively, $u_{ref} = 10\,m/s$ and $z_{ref} = 10\,m$. The aerodynamic roughness considered is $z_0 = 0.0024\,m$ (Nield *et al.*, 2013). Since the analyses consider flat terrain without obstacles, the vertical displacement adjustment parameter was set as $d = 0\,m$. The velocity profile $u(z)$ and the friction velocity, u^*, for the inlet are given by Eq. (5)-(6), respectively, where $\kappa = 0.40$ is the von Kárman constant.

$$u(z) = \frac{u^*}{\kappa} \ln\left(\frac{z-d+z_0}{z_0}\right) \tag{5}$$

$$u^* = \frac{u_{ref}\kappa}{\ln\left(\frac{z_{ref}+z_0}{z_0}\right)} \tag{6}$$

Modeling of the inlet TKE is given by Eq. (7), where $C_1 = 0$ and $C_2 = 1$ are constants for fitting to the ABL profile. For the $k-\epsilon$ closure model, the inlet condition is given by Eq. (8). For the $k-\omega$ SST model, the condition proposed by Yang *et al.* (2009), also expressed by Eq. (9) is considered.

$$k = \frac{(u^*)^2}{\sqrt{C_\mu}} \sqrt{C_1 \ln\left(\frac{z-d+z_0}{z_0}\right) + C_2} \tag{7}$$

$$\epsilon = \frac{(u^*)^3}{\kappa(z-d+z_0)} \sqrt{C_1 \ln\left(\frac{z-d+z_0}{z_0}\right) + C_2} \tag{8}$$

$$\omega = \frac{u^*}{\kappa\sqrt{C_\mu}} \frac{1}{z-d+z_0} \tag{9}$$

On the outlet face, the Neumann condition of zero gradient is considered, i.e., $\nabla\phi \cdot \boldsymbol{n} = 0$, to extrapolate the values of nearby volumes to the downstream of the domain. For the lateral and upper faces, symmetry planes are considered. To represent the buildings in the domain, wall functions are used.

The initial conditions associated with the differential equations that model TKE and dissipation are based on the work of Launder and Spalding (1974), where isotropic turbulence is considered. Finally, the initial condition for the specific dissipation in the simulations with $k-\omega$ SST closure model is modeled according to Menter *et al.* (2003).

3.3 Numerical schemes and mesh refinement

To solve the simulation cases, the simpleFoam utility was used. For the numerical strategies, the time scheme defines how a property is integrated over time. The implicit Euler time scheme was adopted. For the gradient terms, central differentiation through the Gauss linear function was used. This condition limits the gradient, ensuring that the value extrapolated on the faces is restricted to the value of the neighboring cells. For divergence, two terms of velocity advection and of a diffuse nature are used, through the Gauss linear upwind model. The divergence is applied with respect to the volumetric flow (ϕ), velocity, TKE and its dissipation to represent the advection terms. The Laplacian terms are discretized according to the Gauss linear corrected scheme, characterized by a second-order linear interpolation.

The mesh was generated using the blockMesh and snappyHexMesh tools. The first generate a structured mesh and the second refines the volumes near specific objects or regions of the original mesh. In this case, the meshes are refined around the buildings, at the inlet region, and in the wake region where turbulence is generated due to aerodynamic interactions between the solid objects and the flow, as shown in Figure 2. This mesh generation model is commonly employed in computational wind engineering studies.

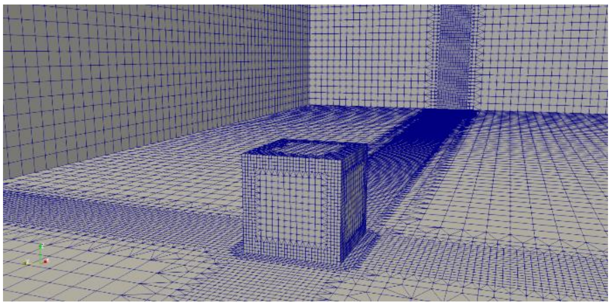

Figure 2: Mesh refinement.

3.4 Aerodynamic coefficients

The calculation of forces is performed considering two components relative to the surface of the analyzed structures: the normal pressure force ($\boldsymbol{F}_p$) on the faces and the tangential viscous force ($\boldsymbol{F}_v$). These are computed using Eqs. (10) and (11), respectively.

$$\boldsymbol{F}_p = \sum_i \rho_i \boldsymbol{s}_{f,i}\left(p_i - p_{ref}\right) \tag{10}$$

$$\boldsymbol{F}_v = \sum_i \boldsymbol{s}_{f,i} \cdot (\mu \boldsymbol{R}_{dev}) \tag{11}$$

where $\rho = 1.225\ kg/m^3$ is the air density, $\boldsymbol{s}_{i,f}$ is the face area vector, p is the pressure, p_{ref} is the reference pressure set as 0 Pa, μ is the dynamic viscosity and $\boldsymbol{R}_{dev}$ is the deviatoric stress tensor.

The sum of these force components is used to calculate the drag, lift and torsion coefficients. The drag direction is assigned to the X-axis, while the reference axes for moment and lift direction are assigned to the Z-axis. Consequently, the coefficients are computed according to Eq. (12).

$$C_D = \frac{F_x}{\frac{1}{2}\rho U_\infty^2 S_a} \qquad C_T = \frac{M_z}{\frac{1}{2}\rho U_\infty^2 S_b L} \qquad C_L = \frac{F_z}{\frac{1}{2}\rho U_\infty^2 S_b} \tag{12}$$

where C_D, C_T and C_L are the aerodynamic coefficients of drag, torque and lift, respectively, F_i and M_i represent the forces in the i directions, $U_\infty = 10\ m/s$ is the reference velocity, L is the reference length of the building's base, S_a is the reference area in the drag direction, and S_b is the reference area for the base. Finally, the average pressure coefficients are obtained using Eq. (13).

$$C_p = \frac{p - p_{ref}}{\frac{1}{2}\rho U_\infty^2} \tag{13}$$

4 VALIDATION

To validate the simulation models in this work, the example of flow around a cube (Martinuzzi and Tropea, 1993) is used. Three finite volume discretizations are employed, M1 (119,342 cells), M2 (382,635 cells) and M3 (885,828 cells).

The pressure coefficients are compared with experimental and numerical results from the literature. They are compared with the results of Richards *et al.* (2001) and Richards *et al.* (2007), who respectively, carried out the experimental test on a cube with a 6 m edge and replicated the results in wind tunnel tests, Lim *et al.* (2009), who carried out an experimental and numerical study using the LES model, Hu *et al.* (2018), who performed numerical and experimental studies on a 6 m silsoe cube, and Gough *et al.* (2019), who compared results in experimental tests in a wind tunnel with numerical results using a hybrid RANS-LES model.

The pressure coefficients are presented in Figures 3-4, which show, respectively, the results of the 3 meshes in the $k-\epsilon$ and $k-\omega$ SST models. Table 1 presents the relative difference of the numerical studies compared with the literature results.

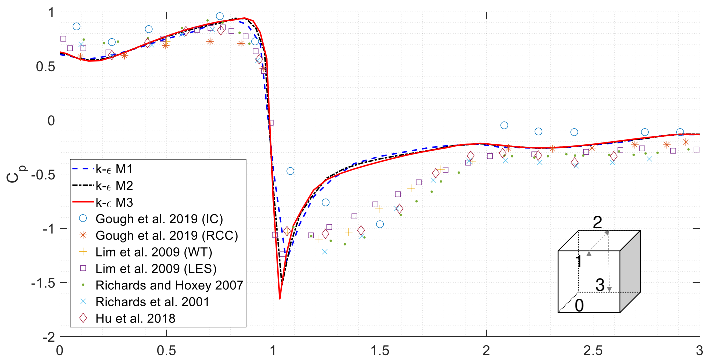

Figure 3: Mean pressure coefficients through the central line of the cube according to $k-\epsilon$ closure model.

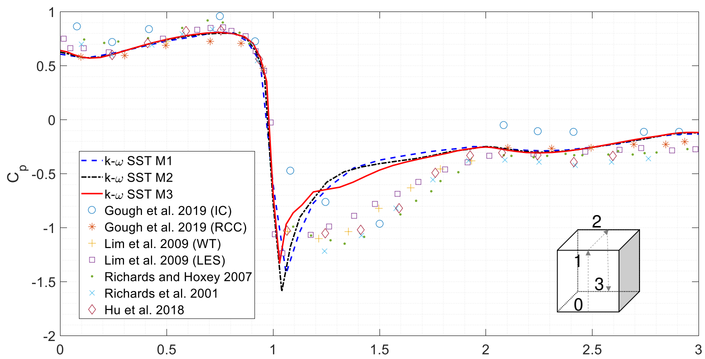

Figure 4: Mean pressure coefficients through the central line of the cube according to $k-\omega$ SST closure model.

The windward, top, and leeward faces of the cube are identified within the intervals [0,1], [1,2] and [2,3], respectively. The results indicate that the RANS models employed in this study

	$k-\epsilon$ (windward)	$k-\epsilon$ (top)	$k-\epsilon$ (leeward)	$k-\omega$ SST (windward)	$k-\omega$ SST (top)	$k-\omega$ SST (leeward)
M1	10,80 %	52,85 %	18,93 %	8,33 %	41,10 %	14,17 %
M2	10,27 %	46,04 %	18,39 %	8,13 %	34,69 %	13,39 %
M3	10,08 %	42,07 %	16,86 %	7,36 %	29,74 %	12,97 %

Table 1: Relative difference of the numerical simulations compared to the literature results.

are more accurate for the windward and leeward faces, with the numerical results aligning closely with experimental and numerical studies in the literature. However, the top face showed the greatest deviation, particularly with the $k-\epsilon$ model. Nevertheless, as seen in Table 1, the results asymptotically converge towards the average of the experimental results, indicating that the employed models are well-suited for faces normal to the wind flow. It is also noteworthy that mesh refinement consistently improves the results, especially on the top face and more significantly with the SST model: the $k-\omega$ SST model on the M3 mesh demonstrated the best agreement with the experimental results.

5 RESULTS

The system evaluated in this work consists of a Commonwealth Advisory Aeronautical Research Council building, or simply CAARC (Melbourne, 1980), which has a base proportion of 1:1.5 and a height of 1:6, and a set of adjacent buildings with a base proportion of 1:1 and a height of 1:3, spaced at a fixed distance, as shown in Figure 5. The evaluated system is subject to wind gusts with an incidence angle ranging from $\theta = 0°$ to 90°, at 15° intervals. The influence of the surroundings on the mean pressure coefficients and on the aerodynamic coefficients of drag, moment and torsion of the CAARC building is studied, comparing it in the isolated configuration and with the neighborhood.

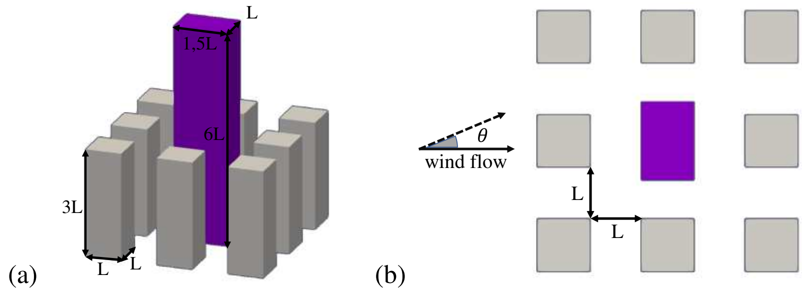

Figure 5: CAARC building and neighborhood: (a) buildings proportions and (b) neighborhood spacing.

Figures 6-8 present the aerodynamic coefficients of the CAARC building in both isolated and surrounded configurations, considering the two turbulence models. It is observed that, in the isolated case, drag and lift reach their maximum values at an incidence angle of $\theta = 45°$, while the torsion coefficient peaks at $\theta = 30°$.

With the addition of the surrounding blocks, there is a substantial reduction in drag. However, in the case of lift, changes in the angle θ cause alterations in the aerodynamic behavior around the building, resulting in values at $\theta \geq 60°$ that are equal or higher than in the isolated case. The formation of vortices within the neighborhood favors the emergence of more intense vertical forces at certain incidence angles, causing lift values to rise compared to the isolated case.

Torsion exhibits a similar behavior in both turbulence closure models, with the surrounding blocks causing a slight decrease in the coefficient. In all cases, the peak occurs at $\theta = 30°$, with

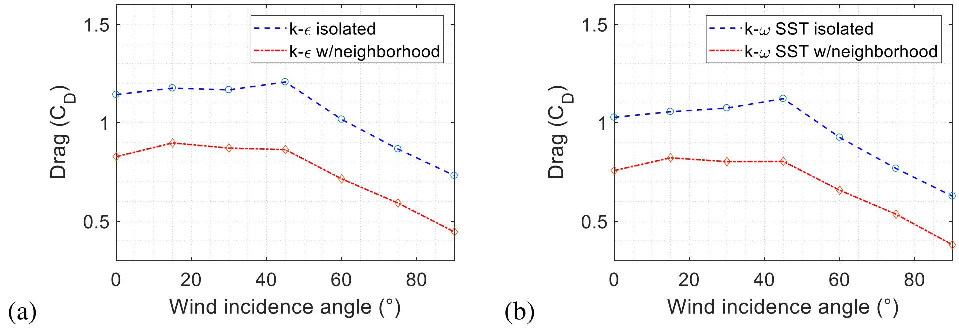

Figure 6: Drag coefficient (C_D): (a) $k - \epsilon$ and (b) $k - \omega$ SST.

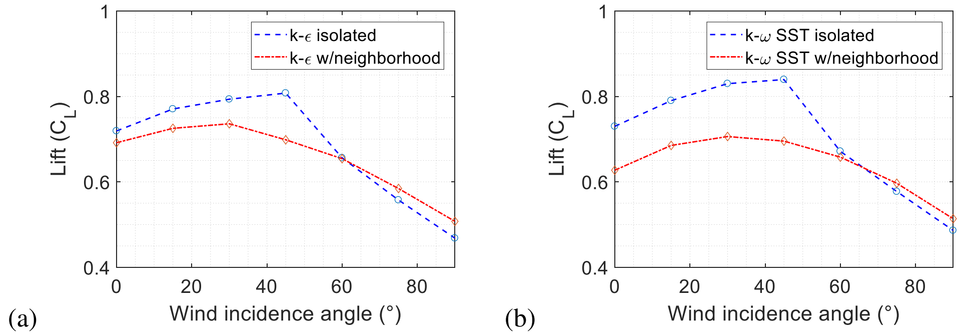

Figure 7: Lift coefficient (C_L): (a) $k - \epsilon$ and (b) $k - \omega$ SST

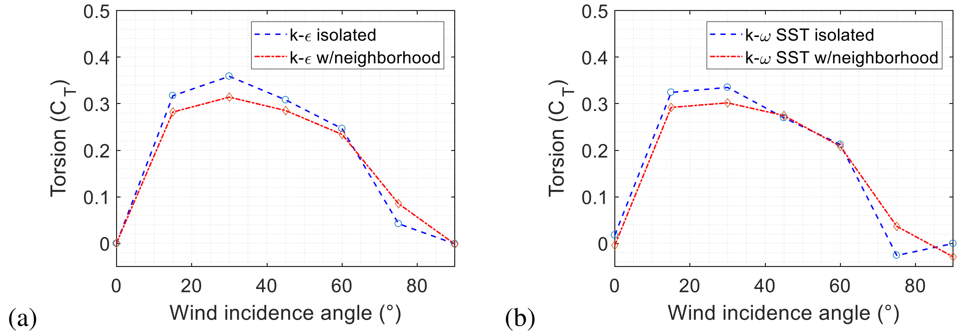

Figure 8: Torsion coefficient (C_T): (a) $k - \epsilon$ and (b) $k - \omega$ SST.

a sharp increase between 0° and 15° and a slight drop between 30° and 90°. Due to the symmetry of the problem, C_T is approximately 0 at $\theta = 0°$ and 90°, with tangential viscous forces accounting for the non-zero values. The results of this study show that intense aerodynamic effects generally occur at non-zero incidence angles. It is important to highlight that the differences in the drag and lift coefficients are due to the rectangular cross-section of the CAARC model, which has an aspect ratio of 1:1.5. Consequently, the coefficients are lower at 90° because the cross-sectional area is smaller.

6 CONCLUSIONS

In this work, Computational Fluid Dynamics simulations were employed to analyze the effects of neighboring structures on the aerodynamic coefficients of the CAARC building model. The RANS methodology was used as the turbulence model, with the closure models $k - \epsilon$ and $k - \omega$ Shear Stress Transport. One of the main points highlighted by the study results is that wind forces acting on buildings reach the highest values when flow did not strike the buildings facades perpendicularly. The aerodynamic coefficients exhibited their highest peaks at different incidence angles. Even with the surrounding buildings shielding the central structure from direct wind exposure, the complexity of aerodynamic behavior indicates that, in the case of lift and torsion coefficients, the intensity of these effects can be amplified.

Despite the simplicity of this study design, which considered a small neighborhood with perfectly aligned buildings, the results reveal complex behaviors in aerodynamic coefficients within urban environment. The use of RANS methodology, reliant on averaged Navier-Stokes equations, introduces certain limitations to the analysis. Additionally, the incidence angles were analyzed with a spacing of 15°; improving the comparison of the results could be achieved by conducting the analysis with 5° spacing. Finally, the actual urban settings present far more intricate building arrangements, and wind patterns exhibit increased complexity in both experimental observations and real-world scenarios.

Nonetheless, this idealized configuration effectively demonstrates how even straightforward cases can exhibit significant aerodynamic complexity, emphasizing the critical role of wind engineering in the design of tall buildings and the planning of urban areas.

ACKNOWLEDGEMENTS

The authors would like to thank the Fundação Coordenação de Aperfeiçoamento de Pessoal de Nível Superior (CAPES) and the Conselho Nacional de Desenvolvimento Científico e Tecnológico (CNPq) for funding this work, and the Pró-reitoria de Pós-graduação (PRPG) from the Federal University of Minas Gerais (UFMG) through the PADO program for covering the expenses related to the conference.

REFERENCES

Andersson, B., Andersson, R., Hakansson, L., Morternsen, M., Sudiyo, R., van Wachem, B. *Computational Fluid Dynamics*, Cambridge University Press, 2012.

Aristodemou, E., Boganegra, L. M., Mottet, L., Pavlidis, D., Constantinou, A., Pain, C., ApSimon, H. How tall buildings affect turbulent air flows and dispersion of pollution within a neighbourhood. *Environ Pollut*, (233):782-796, 2018.

Blocken, B., Janssen, W.D., van Hooff, T. CFD. CFD simulation for pedestrian wind comfort and wind safety in urban areas: General decision framework and case study for the Eindhoven University campus. *Environmental Modelling & Software*, (30):15-34, 2012.

Blocken, B., Stathopoulos, T., van Beeck, J. P. A. J. Pedestrian-level wind conditions around buildings: Review of wind-tunnel and CFD techniques and their accuracy for wind comfort assessment. *Build Environ*, (100):50-81, 2016.

Dondapati, R.S., Rao, V.V. Influence of mass flow rate on Turbulent Kinetic Energy (TKE) distribution in Cable-In-Conduit Conductors (CICCs) used for fusion grade magnets. *Fusion Eng Des*, 88(5):341-349, 2013.

Franke, J., Hirsch, C., Jensen, A.G., Krüs, H.W., Schatzmann, M., Westbury, P.S., Miles, S.D., Wisse, J.A., Wright, N.G., Recommendations on the use of CFD in wind engineering. In: *Proc Int Conf Urban Wind Eng Build Aerodyn*, 2004, Sint-Genesius-Rode, Bélgica, 2004.

Gough, H., King, M.F., Nathan, P., Grimmond, C.S.B., Robins, A., Noakes, C.J., Luo, Z., Barlow, J.F. Influence of neighbouring structures on building façade pressures: Comparison between full-scale, wind-tunnel, CFD and practitioner guidelines. *J Wind Eng Ind Aerod*, (189): 22-33, 2019.

Hargreaves, D.M., Wright, N.G. On the use of the k–ε model in commercial CFD software to model the neutral atmospheric boundary layer. *J Wind Eng Ind Aerod*, 95(5):355–369, 2007.

Hu, J., Xuan, H.B., Kwok, K.C.S., Zhang, Y., Yu. Y. Study of wind flow over a 6 m cube using improved delayed detached Eddy simulation. *J Wind Eng Ind Aerod* 179:463-474, 2018.

Iqbal, Q. M. Z., Chan, A. L. S. Pedestrian level wind environment assessment around group of high-rise cross-shaped buildings: Effect of building shape, separation and orientation. *Build Environ*, (101): 45-63, 2016.

Ishida, Y., Yoshida, A., Kamata, S., Yamane, Y., & Mochida, A. Wind Tunnel Experiments on Interference Effects of a High-Rise Building on the Surrounding Low-Rise Buildings in an Urban Block. *Wind*, 3(1): 97-114 2023.

Ishida, Y., Yoshida, A., Yamane, Y., & Mochida, A. Impact of a single high-rise building on the wind pressure acting on the surrounding low-rise buildings. *J Wind Eng Ind Aerod*, (250): 105742, 2024.

Launder, B.E., Spalding, D.B. The numerical computation of turbulent flows. *Comput Methods Appl Mech Eng*, 3(2):269–289, 1974.

Lim, H. C., Thomas, T. G., Castro, I. P. Flow around a cube in a turbulent boundary layer: LES and experiment. *J Wind Eng Ind Aerod*, 97(2), 96-109, 2009.

Lin, N., Letchford, C., Tamura, Y., Liang, B., Nakamura, O. Characteristics of wind forces acting on tall buildings." *J Wind Eng Ind Aerod*, 93(3):217-242, 2005.

Martinuzzi, R., & Tropea, C. (1993). The flow around surface-mounted, prismatic obstacles placed in a fully developed channel flow (data bank contribution). *J. Fluids Eng.*, 115(1):85-92, 1993.

Meng, F. Q., He, B. J., Zhu, J., Zhao, D. X., Darko, A., Zhao, Z. Q. Sensitivity analysis of wind pressure coefficients on CAARC standard tall buildings in CFD simulations. *J Build Eng*, (16): 146-158, 2018.

Melbourne, W. H. Comparison of measurements on the CAARC standard tall building model in simulated model wind flows. *J Wind Eng Ind Aerod*, 6(1):73-88, 1980.

Menter F.R., Kuntz, M., Langtry, R. Ten years of industrial experience with the SST turbulence model. In: *Proc 4th Int Symp Turbul Heat Mass Transf*, 625–632, Antalya, Turkey, 2003.

Nield, J. M., King, J., Wiggs, G. F., Leyland, J., Bryant, R. G., Chiverrell, R. C., Washington, R. Estimating aerodynamic roughness over complex surface terrain. *JGR: Atmospheres*, 118(23):12-948, 2013.

Razak, A., Hagishima, A., Ikegaya, N., & Tanimoto, J. Analysis of airflow over building arrays for assessment of urban wind environment. *Build Environ*, (59):56-65, 2013.

Richards, P.J., Hoxey, R.P. Appropriate boundary conditions for computational wind engineering models using the k-ε turbulence model. In: *Comput Wind Eng*, 1:145–153. Elsevier, 1993.

Richards, P. J., Hoxey, R. P., Short, L. J. Wind pressures on a 6 m cube. *J Wind Eng Ind Aerod*, 89(14-15), 1553-1564, 2001.

Richards, P. J., Hoxey, R. P., Connell, B. D., Lander, D. P. Wind-tunnel modelling of the Silsoe Cube. *J Wind Eng Ind Aerod*, 95(9-11), 1384-1399, 2007.

Reynolds, O. On the dynamical theory of incompressible viscous fluids and the determination of the criterion. *PTMSFB*, 186:123-164, 1895.

Tominaga Y., Mochida, A., Yoshie, R., Kataoka, H., Nozu, T., Masaru, Y., Shirasawa, T. AIJ guidelines for practial applications of CFD to pedestrian wind environment around buildings. *J Wind Eng Ind Aerod*, 96:1749-1761, 2008.

Thepmongkorn, S., Wood, G. S., Kwok, K. C. S. Interference effects on wind-induced coupled motion of a tall building. *J Wind Eng Ind Aerod*, 90(12):1807-1815, 2002.

Van Doormaal, J.P., Raithby, G.D. Enhancements of the SIMPLE Method for Predicting Incompressible Fluid Flows. *Numer Heat Transf*, 7(2), 1984.

Yang, Y., Gu, M., Chen, S., Jin, X. New inflow boundary conditions for modelling the neutral equilibrium atmospheric boundary layer in computational wind engineering. *J Wind Eng Ind Aerod*, 97(2):88–95, 2009.